

---

# SEGMENTING WHITE MATTER HYPERINTENSITIES ON ISOTROPIC THREE-DIMENSIONAL FLUID ATTENUATED INVERSION RECOVERY MAGNETIC RESONANCE IMAGES: A COMPARISON OF DEEP LEARNING TOOLS ON A NORWEGIAN NATIONAL IMAGING DATABASE

---

A PREPRINT

## **Røvang, Martin Soria\***

Computational Radiology & Artificial Intelligence (CRAI) -,  
Division of Radiology and Nuclear Medicine, Oslo University Hospital, Oslo, Norway  
Division of Medicine and Laboratory Sciences, University of Oslo, Oslo, Norway  
m.s.rovang@medisin.uio.no

## **Selnes, Per**

Department of Neurology, Akershus University Hospital, Lørenskog, Norway  
Institute of Clinical Medicine, Campus Ahus, University of Oslo, Oslo, Norway

## **MacIntosh, Bradley John**

Computational Radiology & Artificial Intelligence (CRAI) -,  
Division of Radiology and Nuclear Medicine, Oslo University Hospital, Oslo, Norway  
Department of Medical Biophysics, University of Toronto, Toronto, Canada  
Sandra Black Centre for Brain Resilience & Recovery, Hurvitz Brain Sciences Program,-  
Physical Sciences Platform, Sunnybrook Research Institute, Toronto, Canada

## **Groote, Inge Rasmus**

Computational Radiology & Artificial Intelligence (CRAI) -,  
Division of Radiology and Nuclear Medicine, Oslo University Hospital, Oslo, Norway  
Department of Radiology, Vestfold Hospital Trust, Tønsberg, Norway

## **Pålhaugen, Lene**

Department of Neurology, Akershus University Hospital, Lørenskog, Norway  
Institute of Clinical Medicine, Campus Ahus, University of Oslo, Oslo, Norway

## **Sudre, Carole**

School of Biomedical Engineering and Imaging Sciences, King's College London, London, UK.  
Dementia Research Centre, Institute of Neurology, University College London, London, UK  
Department of Medical Physics, University College London, London, UK.

## **Fladby, Tormod**

Department of Neurology, Akershus University Hospital, Lørenskog, Norway  
Institute of Clinical Medicine, Campus Ahus, University of Oslo, Oslo, Norway

## **Bjørnerud, Atle**

Computational Radiology & Artificial Intelligence (CRAI) -  
Division of Radiology and Nuclear Medicine, Oslo University Hospital, Oslo, Norway.  
Department of Physics, University of Oslo, Oslo, Norway

## SUMMARY

**Introduction** Automated segmentation of white matter hyperintensities (WMHs) is an essential step in neuroimaging analysis of Magnetic Resonance Imaging (MRI). Fluid Attenuated Inversion Recovery (FLAIR-weighted) is an MRI contrast that is particularly useful to visualize and quantify WMHs, a hallmark of cerebral small vessel disease and Alzheimer's disease (AD). Clinical MRI protocols migrate to a three-dimensional (3D) FLAIR-weighted acquisition to enable high spatial resolution in all three voxel dimensions. The current study details the deployment of deep learning tools to enable automated WMH segmentation and characterization from 3D FLAIR-weighted images acquired as part of a national AD imaging initiative.

**Materials and methods** An off-the-shelf 3D model from the nnU-Net framework and an in-house developed 2.5D U-Net model were trained and validated on data from the ongoing Norwegian Disease Dementia Initiation (DDI) multicenter study. A third state-of-the-art Deep Bayesian network model (HyperMapp3r) was implemented without de-novo tuning, to serve as an architecture for comparison.

Among 642 participants (283 male, mean age: (65.18 +/- 9.33) years) from the DDI study, the two in-house networks were trained and validated across five national collection sites. All three models were tested on a held-out subset of the internal data from the 642 participants and an external dataset with 29 cases from an international collaborator. These test sets were evaluated independently. Five established WMH performance metrics were used for comparison against ground truth human-in-the-loop segmentation.

**Results** Of the three networks tested, the 3D nnU-Net had the best performance with an average dice similarity coefficient score of 0.78 +/- 0.10, performing better than both the in-house developed 2.5D model and the SOTA Deep Bayesian network.

**Conclusion** With the increasing use of 3D FLAIR-weighted images in MRI protocols, our results suggest that WMH segmentation models can be trained on 3D data and yield WMH segmentation performance that is comparable to or better than state-of-the-art without the need for including T1-weighted image series. The 3D nnU-Net gave the overall best performance and will be used for further testing on new data and automating WMH segmentation in our ongoing AD-related research activities.

**Keywords** White matter hyperintensities · Brain lesions segmentation · U-Net · Magnetic resonance imaging · Deep Bayesian Networks

---

<sup>0</sup>WMH - White Matter Hyperintensities, PET - Positron Emission Tomography, SVD - Cerebrovascular small vessel disease, AD - Alzheimer's disease, FLAIR - Fluid Attenuated inversion recovery, MICCAI - Medical Image Computing and Computer-assisted Intervention, MRI - Magnetic Resonance Imaging, DSC - Dice similarity coefficient, HD95 Hausdorff Distance 95th percentile, AVD - Average Volume Difference, SOTA - State-Of-The-Art, DDI - Disease Dementia Initiation, 3D - 3-dimensional, TP - True Positives, FN - False Negatives, FP - False Positives, AI - Artificial Intelligence, STAPLE - Simultaneous truth and performance level estimation, IQR - Interquartile Range, MONAI - Medical Open Network for Artificial Intelligence

## 1 Introduction

Alzheimer's disease (AD) is the most common type of dementia and is characterized by the deposition of neuro-toxic amyloid plaques in the cerebral cortex[1]. Amyloid plaques can be detected by (amyloid) Positron Emission Tomography (PET) or measurement of amyloid- $\beta$  species in the cerebrospinal fluid. Cerebrovascular small vessel disease (SVD) is an independent driver of dementia and the co-pathologies seen between AD and SVD[2].

Subcortical white matter hyperintensities (WMHs) of presumed vascular origin on T2-weighted MRI is an established surrogate marker for SVD[3], but WMHs are also considered a core feature of AD[4]. Quantifying WMH lesion load through segmentation on MRI is relevant pertaining characterization of AD and vascular cognitive impairment. However, this introduces a significant workload in a neuroradiology service, and therefore robust and automated segmentation software tools are desirable[5].

Deep learning has demonstrated clinical value across a wide range of imaging applications[6], including lesion segmentation in MRI. A recent report combined T2-weighted fluid-attenuated inversion recovery (FLAIR-weighted) and T1-weighted images to yield good WMH segmentation performance, arguably a state-of-the-art (SOTA) solution[7].

Other Deep learning-based WMH segmentation publications trained the models using either fully or partly open-source datasets; for example in the Medical Image Computing and Computer-assisted Intervention (MICCAI) WMH segmentation challenge[8].

Open-source data ensures that results can be readily compared, however, it remains to be seen whether new data sources, such as from other MRI systems and sites, will degrade performance. The MICCAI WMH segmentation challenge has dramatically increased research interest and collaboration, and there is a need to extend this work, i.e. build from the 170 participants and six MRI sites.

A general objective is to develop automated WMH detection and quantification tools across a range of MR systems and MRI sequence parameters. A central aspect of this initiative is the early adoption of 3D and isotropic voxel resolution for the FLAIR-weighted sequence. The current study aligns with an ongoing Norwegian nationwide effort aimed at the early detection of AD[9].

The study was motivated by the observation that existing WMH segmentation models are mainly trained on anisotropic 2D FLAIR-weighted images, whereas the national MRI protocol for pre-dementia evaluation in Norway is exclusively based on 3D FLAIR-weighted with (close to) isotropic resolution.

From this, we aimed to investigate several convolutional neural network(CNN) architectures to find the model yielding the best WMH segmentation performance in isotropic resolution FLAIR-weighted images. Two trained networks

were implemented, one of which was developed in-house. Models were trained solely on 3D FLAIR-weighted from the multicenter Norwegian cohort. Performance was compared against the recently published SOTA model, a Deep Bayesian networks model (Hypermapp3r)[10] which was trained on a combination of 2D FLAIR-weighted and 3D T1-weighted images sets.

Lastly, model performances were compared to the results of the MICCAI WMH segmentation challenge from 2019. We hypothesized that the in-house neural networks designed and trained on 3D FLAIR-weighted data would achieve high WMH segmentation performance using a battery of widely accepted performance metrics.

## 2 Materials and Methods

### 2.1 Participants

The study includes MRI image sets from 642 adult participants (283 males), mean age: (65.18 +/- 9.33) years, at the time of enrollment in the longitudinal Norwegian Disease Dementia Initiation (DDI) multicenter study. The DDI study includes five national sites with MRI performed on six different scanners from two different vendors. Details of the study population included are reported previously[11].

In short, individuals who reported cognitive concerns or as assessed by next of kin were recruited mainly by advertisement, from memory clinics, or from a previous study. Exclusion criteria were brain trauma or disorder, stroke, previous dementia diagnosis, severe psychiatric disease, a severe somatic disease that might influence cognitive functions, intellectual disability, or developmental disorders.

Age-matched controls were recruited from advertisements or were patients admitted to the hospital for orthopedic surgery. We also included a second cohort of 29 adults that were scanned at a single site in the Czech Republic to serve as an external test set. All participants provided written consent, and the study has been approved by the regional ethics committee (REK SØ 2013/150).

### 2.2 MRI data

3D FLAIR-weighted MR images were acquired at 1.5 T or 3 T. Relevant pulse sequence parameters are provided in Table 1. Table 2 provides the breakdown of data splitting.

### 2.3 Data annotation

Ground truth WMH annotations were generated as previously described [11]. Briefly, initial segmentation estimates were obtained using Gaussian mixture modeling [12]. These automated segmentations were subsequently visually reviewed and approved a by domain expert neurologist (LP). For a subset of the cases, multiple iterations of the Gaussian mixture model were needed to exclude false

Table 1: *Dataset information for the internal dataset. The external dataset uses Prisma only with the same parameters.*

Institution	Model	Software	Field Strength	Repetition Time (msec)	Echo Time (msec)	Flip Angle (deg)	Resolution (x,y,z) (mm)
Institution 1	Avanto	syngo_MR_B19	1.5	1700	2.42	15	(1.2,1.05,1.05)
Institution 2	Avanto	syngo_MR_B19	1.5	1700	2.42	15	(1.2,1.04, [1.0,1.04])
Institution 3	Avanto	syngo_MR_B19	1.5	1700	2.42	15	(1.2,1.05,1.05)
Institution 4	Avanto	syngo_MR_B19	1.5	1180	4.36	15	(1.0, 1.0, 1.0)
Institution 5	Ingenia	[5.1.7,5.3.0.3]	3.0	[4.47, 4.91]	[2.218, 2.431]	8	([1.0, 1.2], 1.2, 1)
Institution 6	Prisma	syngo_MR_E11	3.0	2200	1.47	8	(1.0, 1.0, 1.0)
Institution 7	Skyra	syngo_MR_E11	3.0	2300.0	2.98	9	(1.2, 1.0, 1.0)
Institution 8	Prisma	syngo_MR_E11	3.0	2200	1.47	8	(1.0, 1.0, 1.0)
Institution 8	Ingenia	[5.1.7, 5.1.7.2]	3.0	[4.48, 4.92]	[2.225, 2.45]	8	([1.0, 1.2], 1.0, 1.0)
Institution 9	Skyra	syngo_MR_D113C	3.0	2300	2.98	9	(1.2, 1.0, 1.0)
Institution 10	Achieva	[3.2.1, 3.2.1.1]	3.0	[6.36, 6.72]	[3.02, 3.14]	8	([1.0, 1.2], 1.0, [1.0, 1.01])
Institution 11	Ingenia	[5.1.2, 5.1.7, 5.1.7.2]	1.5	[7.47, 7.90]	[3.40, 3.68]	8	(1.0, 1.0, 1.0)
Institution 12	Optima MR450w	[DV25.0_R01_1451.a, DV25.1_R03_1802.a]	1.5	[11.24, 11.38]	[5.0, 5.05]	10	(1.2, [1.0, 1.04], [1.0, 1.04])
Institution 13	Skyra	[syngo_MR_D113C, syngo_MR_E11]	3.0	2300	[2.97, 2.98]	9	(1.2, [1.0, 1.01], [1.0, 1.01])
External Institution 1	Prisma	syngo_MR_E11	3.0	2200	1.47	8	(1.0, 1.0, 1.0)

Table 2: *Split of MRI cases for training, validation, and testing across the different MR systems included for the 2.5D model. Avanto and Optima MR450 are 1.5 Tesla systems and the remaining 3 Tesla systems.*

Data split	Skyra	Prisma	Ingenia	Optima MR450w	Achieva	Avanto
Training n=466	47	22	247	84	49	17
Validation n=116	10	6	53	23	18	6
Test (Internal) n=60	5	3	30	12	8	2
Test (External) n=29	-	29	-	-	-	-

positives and a consensus review with a second neurologist (PS) was performed for cases with uncertain ground truth.

## 2.4 Network architectures

The two prototype networks were 2.5D- and 3D nnU-Net models trained on the Norwegian cohort 3D FLAIR-weighted data. The former is a model developed in-house and referred to as 2.5D, to denote the role that neighboring slices/views contribute to the training and inference[13]. The latter is the nnU-Net which has shown promising results for many different medical image segmentation problems[14].

A third model was also considered in this study; the Deep Bayesian networks(we will call this Deep Bayesian going forward), also called the Hypermapp3r model, which has recently been described and was considered a state-of-the-art WMH segmentation tool. Here, the Deep Bayesian was implemented “off the shelf”, and was previously trained on two image inputs (i.e. 3D T1- and 2D FLAIR-weighted images), and no de-novo network training was performed for the current study.

**1) 2.5D U-Net** We used a 256x256 U-Net architecture[15] with encoding feature map sizes of [32, 64, 256, 512]. Each convolution block used the Mish activation function[16]. The upsampling in the decoding layers consisted of transposed convolutions[17]. Using a 2.5-dimensional U-Net configuration, three adjacent 3D FLAIR-weighted slices were used as input as separate channels, with a prediction

done on the center channel. This model had a total of 7.8M parameter estimates and was developed in Pytorch[18].

**2) 3D nnU-Net** A 3D DynUNet from the Medical Open Network for Artificial Intelligence (MONAI) python library[19] was used as implemented in the 3D nnU-Net NVIDIA NGC catalog [20] V. 21.11.0, where “nn” stands for “no new” to denote a widely used and standardized U-Net implementation. We used default parameters for this model. The encoding feature map sizes were [32, 64, 128, 256, 320, 320]. nnU-Net is a self-adapting framework and includes a series of network optimization and pre-processing steps. This model had a total of 31.2M parameter estimates and was developed in Pytorch.

**3) Reference model: Deep Bayesian model (HyperMapp3r)** This comparison model is described as a Deep Bayesian using a 3D CNN based on the U-Net structure with Monte-Carlo dropout at each encoding layer; the dropout layers allow for confidence intervals to be estimates of uncertainty along with the predicted segmentation. The encoding feature map sizes were [16, 32, 64, 128, 256] and had a total of 515k parameter estimates. This Model was developed in Keras [21][22].

## 2.5 Data pre-processing

Data were converted from Digital Imaging and Communications in Medicine (DICOM®) to Neuroimaging Informatics Technology Initiative (NIfTI) files. For the in-house model training, images were intensity bias-corrected us-

ing the N4 algorithm[23], all values below zero were set to zero and subsequently z-normalized by subtracting the mean intensity across volume from each voxel and dividing by the corresponding intensity standard deviation. Then, 1/12 of the slices from each plane were removed to decrease the amount of empty/non-informative slices used during training.

For the 2.5D U-Net model training, data separation into training and validation was done using the NumPy[24] choice function with random seed 1, whereas the 3D nnU-Net used a built-in data separation function. The test data were sampled using Pandas[25] sample function and were sampled in such a way that the test data contained 10% of the total data from each scanner.

Lesions below five voxels in diameter were considered to represent noise and/or non-significant lesions and were removed from the data[26] using the diameter\\_opening morphology function from scikit-image[27]. For context, the pre-processing steps described in the Deep Bayesian model included N4 bias correction and skull-stripping for separating the brain from non-brain tissues[28], and z-normalization of the segmented brain volumes.

## 2.6 Training & Validation

**1) 2.5D U-Net** The loss and evaluation metrics were calculated by first finding the loss and scores in a mini-batch, which comprised of 8x3 individual slices that were sliced from all three orthogonal planes of the MRI volumes from four randomly sampled scan volumes. These slices were also online augmented with horizontal and vertical flips (probability 0.3) and image shearing with (-0.087-0.087) radians, scaling of (0.9-1.1), and rotation of (-0.26-0.26) radians, all with a probability of 0.1. The mini-batch array was flattened along the slice axis and Tversky focal loss[29] is shown in Equation 1,

$$\left(1 - \frac{TP + \Omega}{TP + \alpha FN + \beta FP + \Omega}\right)^\gamma \quad (1)$$

with  $\gamma = 4/3$  and a smoothing factor  $\Omega = 1$  was used as loss function. This loss function is a generalized Dice similarity coefficient(DSC) loss with an exponential hyperparameter that changes the g examples in the training data. Depending on the  $\gamma$  parameter value, the gradient is higher for the gradient from a linear to an exponential loss, causing the gradient to saturate for the easy examples that get scores closer to zero, and are saturating towards a higher score. This forces the network to focus more on difficult examples in the training data. The model weights were saved when the validation data had the highest  $F_2$  score, defined by  $\beta = 2$  and with smoothing factor  $\Omega = 1$  in the generalized F score given in Equation 2

$$\frac{(1 + \beta^2)TP + \Omega}{(1 + \beta^2)TP + FP\beta^2FN + \Omega} \quad (2)$$

To maintain the same size after convolution, images were expanded using zero padding. After all mini-batches for

the epoch were completed, the result was the average over all the mini-batch step results. The  $F_2$  scores were only calculated for the validation set. During the evaluation, the weights were saved at maximum  $F_2$ . The model was trained for 31 epochs and then stopped manually, since the validation metric was found to plateau and remain stable for >9 epochs.

The initial learning rate was  $\eta = 0.0001$ . A learning rate scheduler reduced the learning rate by a factor of 0.2 every five plateau epochs. If the validation loss did not decrease for five epochs, the learning rate was reduced. A mini-batch size of 8x3 random slices was used, with eight slices taken from three orientations of the volume.

We use an Adam optimizer[30] with parameters: betas = (0.9,0.999) eps =  $e^{-8}$  and weight decay = 0. The weights were initialized with a uniform distribution,  $\mathcal{U}(-\sigma_N, \sigma_N)$ , where  $\sigma_N = 1/\sqrt{N}$ , and  $N$  is the size of the layer. The MONAI function "set determinism" with seed 0 and "None" as additional settings were used for reproducibility.

**Prediction during inference with Simultaneous truth and performance level estimation Simultaneous truth and performance level estimation (STAPLE)** is an algorithm that was originally developed to estimate a single maximum likelihood segmentation from multiple independent segmentations of the same object [31]. For the 2.5D U-Net model, one prediction for each plane was made, so we had three prediction volumes based on each of the planes. Then, the STAPLE method was used during inference to obtain a single maximum likelihood segmentation from individual segmentations inferred from three orthogonal planes.

**2) 3D nnU-Net** The 3D nnU-Net model was trained on the same data as the in-house 2.5D U-Net model, but with a different training and validation subset configuration, as it used cross-validation with its own randomness setup. For the training and validation procedure, only one fold (fold=0) was used, with an 80/20 training/validation split.

The pre-processing pipeline consisted of cropping the region of non-zero values, resampling to the median voxel spacing of their respective dataset (with the exception of anisotropic datasets, where the lowest resolution axis was selected to be the 10th percentile of the spacings), padding volumes so that the dimensions were equal to a patch size of (128,128,128) and z-score normalization.

Augmentation included oversampling the foreground class, mirroring, zooming, Gaussian noise, Gaussian blur, brightness, and contrast. The framework also used mixed-precision during training. For testing, the model used test time augmentation (TTA) which has been shown to improve results[32].

The loss function was a sum of DSC and cross-entropy losses. The weights with the highest DSC score on the validation data were saved and used for the test data. This model is very optimized and was able to train for 574

epochs and stopped training when the validation score did not increase for 100 epochs.

### 3) Deep Bayesian (Hypermapp3r) comparison model

We ran this comparison model exclusively on the test datasets and used "out of the box" pre-trained weights. The model was trained using an augmentation scheme that consisted of four transformations: Flipping along the horizontal axis, random rotation by an angle  $+/ - 90$  along the  $y$  and  $z$  axes, and the addition of Rician noise generated by applying the magnitude operation to images with added complex noise, where each channel of the noise is independently sampled from a Gaussian distribution with random  $\sigma = (0.001, 0.2)$  and changing Image intensity by  $\gamma = (0.1, 0.5)$ .

Since this model requires a brain mask, the test data was segmented using the HD-BET segmentation tool[33]. To infer our data using the Deep Bayesian model, we called the batch command for their software "seg\_wmh" with the path for FLAIR-weighted images, T1-weighted images, and a brain mask.

This model used two input channels FLAIR-weighted and T1-weighted compared to the in-house models which only used one FLAIR-weighted image input. During inference, the model generated twenty predictions per participant to develop an uncertainty map of the segmentation.

## 2.7 Test metrics

We used the following metrics on the test datasets, chosen to align with results from the MICCAI WMH challenge:

- Dice similarity coefficient (DSC)[34].
- Hausdorff distance[35] (HD95, modified, 95th percentile in mm). For this metric, smaller values represent better performance.
- Average volume difference (AVD, in percentage). For this metric, smaller values represent better performance.
- Recall for individual lesions[36]
- $F_1$ -score for individual lesions[37]

The implementation of these metrics was found on the MICCAI WMH challenge website.

## 2.8 Test statistics

The implementation of these metrics was found on the MICCAI WMH challenge website. Since performance metrics in the test dataset, in general, were not found to be normally distributed using the Shapiro-Wilk test, we used non-parametric test statistics.

Friedman's related samples Analysis of Variance (ANOVA) by ranks was used to test the null hypothesis that the distribution of each test metric across subjects was the same for all three models, whereas the alternative hypothesis was that they are not the same. An additional

pair-wise comparison was performed between models. Statistical analyses were performed in SPSS V.28.0 (IBM SPSS Statistics). The significance level was set to  $p=.05$ .

## 3 Results

### 3.1 WMH volume distribution of the data

The distribution of total WMH volumes in the whole internal dataset is shown in Figure 1. The median and the

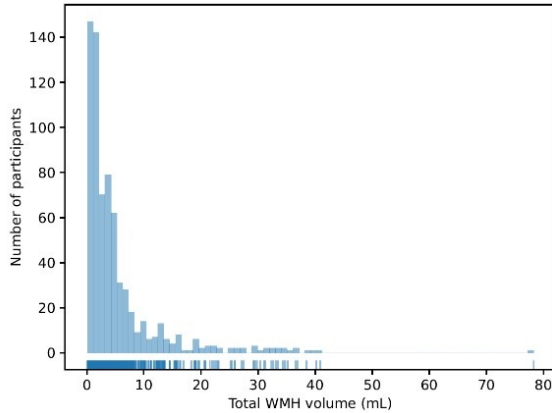


Figure 1: Distribution of total WMH volume per subject in the multi-center internal dataset. The median and interquartile range of the total WMH volume was 2.98(1.29-5.83) mL and the total range (0.11-78.26) mL.

interquartile range(IQR) of the total WMH volume per participant was 2.98(1.29-5.83) mL.

### 3.2 Segmentation results

Validation: in-house trained models The results for the validation data for the two in-house trained models are shown in Table 3.

The performances of both models were lesion size-dependent, with better performance in larger lesions, as summarized in Table 4.

**Test data segmentation results: all three models** The segmentation results for the internal test data are shown in Table 5 together with the best model results from the MICCAI WMH challenge in parenthesis and orange color in the column description.

Overall, there were significant differences in model performance for all metrics and both test sets (Related-Samples Friedman's Two-Way Analysis of Variance by Ranks,  $p<0.001$  for all tests except HD95 for the external test set with  $p=.043$ ). The 3D nnU-Net was found to have the best performance for all metrics compared to 2.5D and Deep Bayesian models. Figures 2 and 3 show boxplots of the five performance metrics for internal and external test sets, respectively.

Table 3: Performance metrics (mean +/- std.dev) for the 2.5D U-Net and 3D nnU-Net in the validation data. Shown is the model used in the experiments and the five metrics used in the white matter hyperintensity challenge for The Medical Image Computing and Computer-Assisted Intervention Society.

Model	DSC	HD95 [mm]	AVD [%]	Recall	$F_1$
2D U-Net	0.70 +/- 0.14	15.04 +/- 15.04	37.89 +/- 33.24	0.47 +/- 0.17	0.59 +/- 0.13
3D nnU-Net	0.78 +/- 0.14	9.15 +/- 16.81	13.70 +/- 14.64	0.71 +/- 0.15	0.72 +/- 0.11

Table 4: Prediction metrics (lesion level) as a function of lesion size for the three models on the validation data. The values are shown as 2.5D U-Net/3D nnU-Net. The threshold set for true positive (TP) and false negatives (FN) is less than 50% of the lesion predicted by the model, otherwise false positive (FP).

Lesion volume range mm <sup>3</sup>	[1, 10]	[10, 400]	[400, 1000]	[1000+ ]
Avg. Volume mm <sup>3</sup>	8/4	70/54	624/621	2872/3353
Total	541/1932	2197/2317	108/110	89/87
Total TP	502/864	1896/2216	107/110	89/87
Total FN	2184/1511	1292/770	2/0	1/1
Total FP	39/1068	301/101	1/0	0/0
Recall	0.18/0.33	0.57/0.65	0.94/0.86	0.96/0.89

Table 5: Performance metrics (mean +/- std.dev) for all three models in the internal test dataset. \*, and ^ indicate that the model performance is significantly better ( $p < 0.05$ ) compared to the 2.5D U-Net and Deep Bayesian respectively. Shown are the results from the five metrics used in the white matter hyperintensity challenge for The Medical Image Computing and Computer-Assisted Intervention Society. The values in the parenthesis are the best results from the WMH challenge.

Model	DSC (0.81)	HD95 [mm] (5.63)	AVD [%] (18.58)	Recall (0.82)	$F_1$ (0.79)
2.5D U-Net	0.70 +/- 0.13	17.02 +/- 15.97	45.04 +/- 51.00	0.50 +/- 0.18	0.59 +/- 0.13
3D nnU-Net	<b>0.78 +/- 0.10</b> * <sup>^</sup>	<b>10.30 +/- 18.24</b> * <sup>^</sup>	<b>16.53 +/- 15.86</b> * <sup>^</sup>	<b>0.72 +/- 0.14</b> * <sup>^</sup>	<b>0.71 +/- 0.10</b> * <sup>^</sup>
Deep Bayesian	0.63 +/- 0.15	17.78 +/- 12.83	43.24 +/- 57.92	0.51 +/- 0.18	0.56 +/- 0.14

For the internal test set, average (+/- std.dev) DSC scores were 0.70 (+/- 0.13), 0.78 (+/- 0.10) and 0.63 (+/- 0.15), for the 2.5D U-Net, 3D nnU-Net and Deep Bayesian models respectively. The corresponding DSC scores for the external test set was 0.54 (+/- 0.19), 0.66 (+/- 0.17) and 0.53 (+/- 0.18).

Figures 4 and 5 show sample cases of segmentation performance for all three models for the internal test set, with the yellow color to denote over-segmentation, red as under-segmentation, and green as correct segmentation. Test performance as a function of lesion size for the three models is shown in Table 6.

As expected, all performance metrics decreased with decreasing lesion size for all three models. Using a threshold at > 50% overlap of the lesion with ground truth for true positive values and grouping lesions according to size range: (1-10, 11-400, 401-1000, 1000+>)mm<sup>3</sup>, gave true positive rates of (18.94, 63.69, 100 and 100)%, (35.23, 74.96, 100 and 100)%, (18.55, 43.34, 84.44 and 96.97)% for the 2.5D U-Net, 3D nnU-Net, and Deep Bayesian, respectively. In Tables 7 and 8, the results for the external test data results are shown.

In the external dataset, the Deep Bayesian model failed to predict >50% overlap for some large lesions, which can also be seen in Figure 6-b.

Figure 7 shows the histogram distribution of FLAIR-weighted image intensity mean and entropy across all volumes in the training and the two test datasets. The difference in intensity distribution between the two test sets is evident and may explain the reduced performance of all three models in the external test set.

## 4 Discussion

In the present study, we evaluated the performance of 2.5D and 3D nnU-Net CNN models for their ability to segment WMH based on volumetrically-acquired FLAIR-weighted MRI sequences across a range of older adults participants and in the context of a multi-center pre-dementia imaging initiative. We compared these architectures against a recently published SOTA Deep Bayesian model.

The present study is novel because it involved a large sample of participants from a national multi-center pre-dementia case-control study where near isotropic 3D FLAIR-weighted images were acquired and for which do-

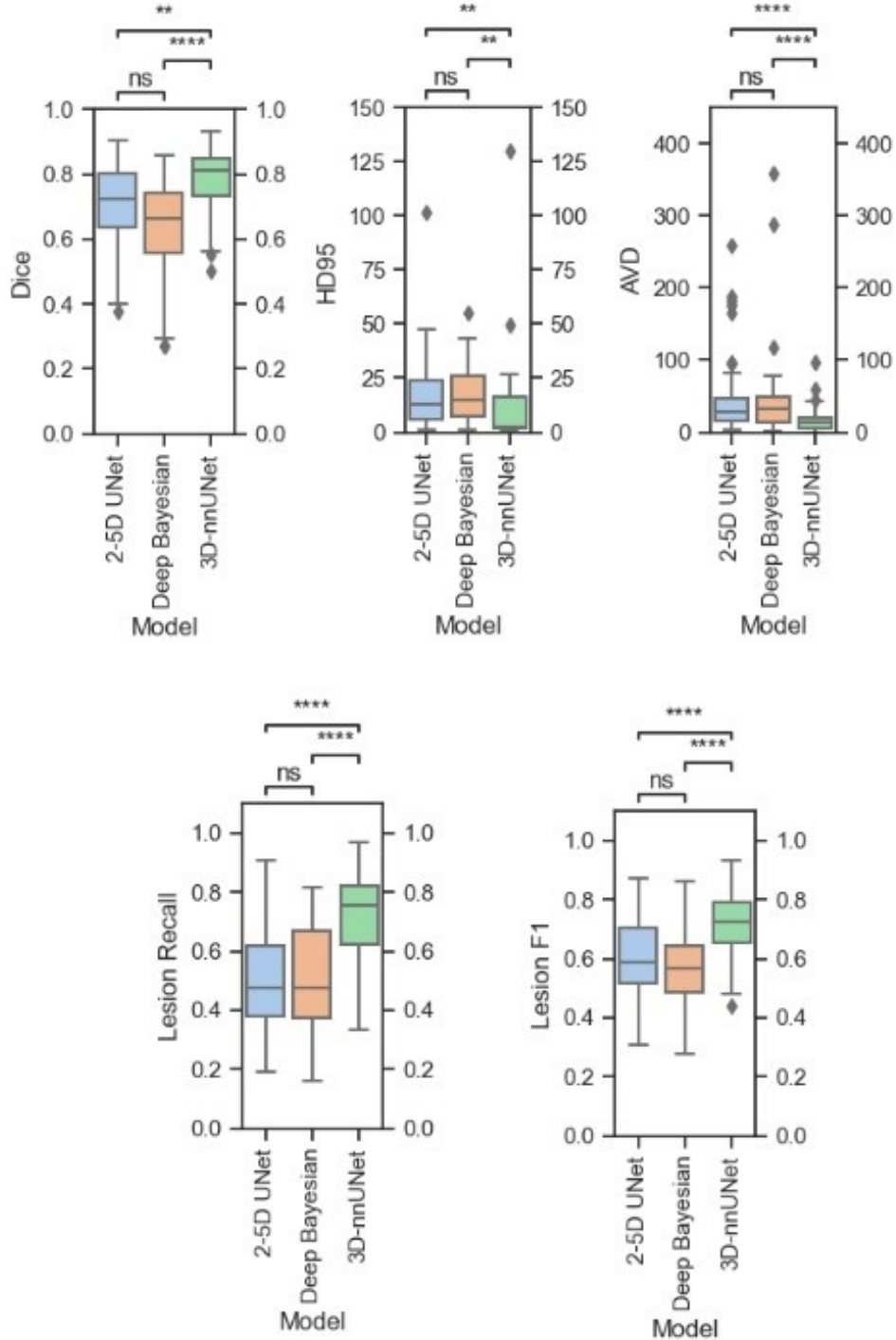


Figure 2: Boxplot of the internal test data ( $n = 60$ ) performance metrics. The 3D nnU-Net is favorable for all metrics, giving the best means for all metrics with a  $p$ -value  $< 0.001$  compared to the other models. The  $p$ -value legends are: ns:  $0.05 < p \leq 1.00$ , \*:  $0.01 < p \leq 0.05$ , \*\*:  $0.001 < p \leq 0.01$ , \*\*\*:  $0.0001 < p \leq 0.001$ , \*\*\*\*:  $p \leq 0.0001$ .

main experts carefully reviewed segmentations to create a robust ground truth.

In larger previous research projects like the WMH challenge and from the Deep Bayesian, the FLAIR-weighted

data were either 2D or resliced into a 2D because of decreased annotation time and to fit the 2D T1-weighted images. Some prior WMH segmentation research used 3D FLAIR images[38][39], but these studies have smaller

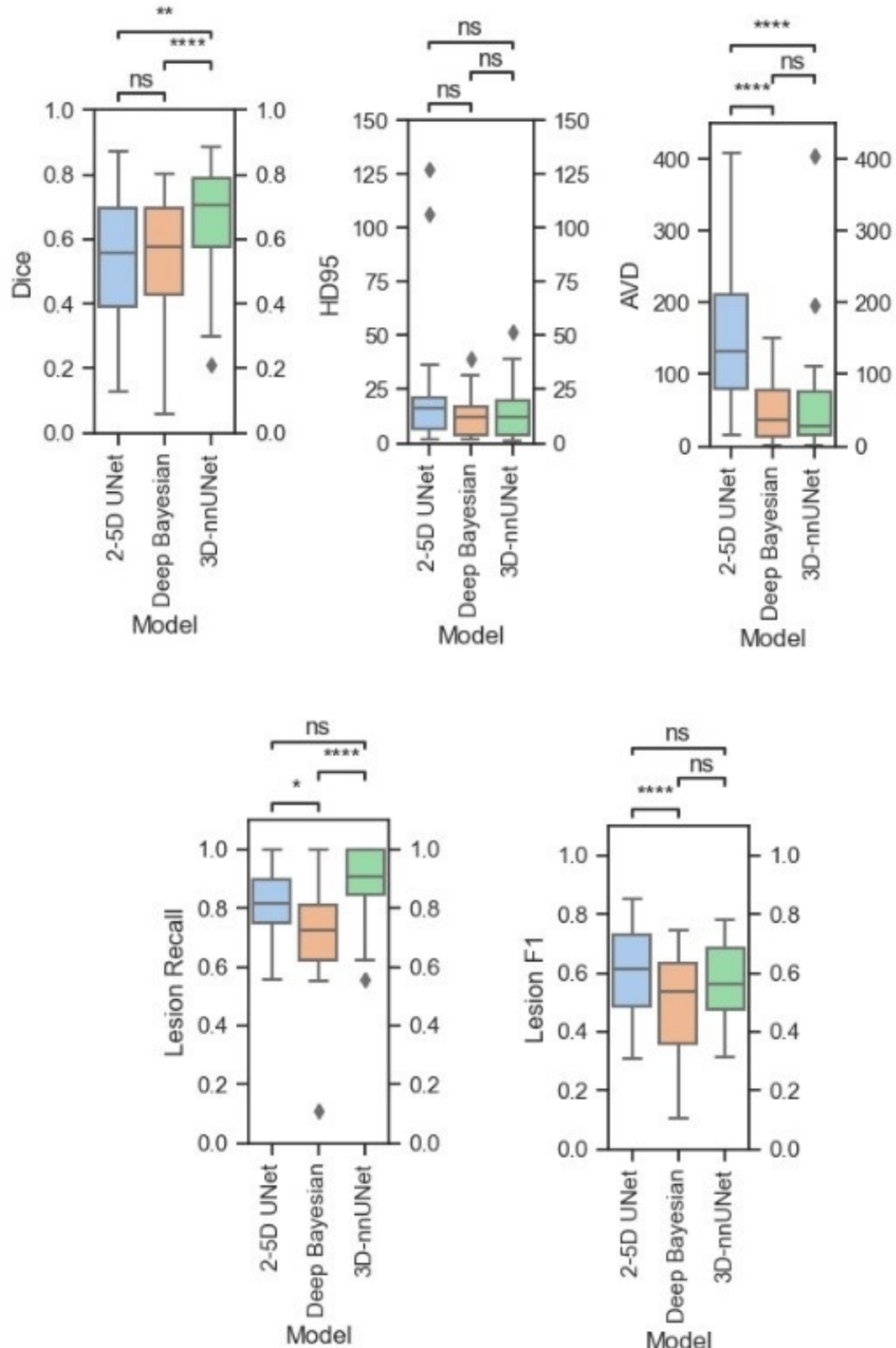
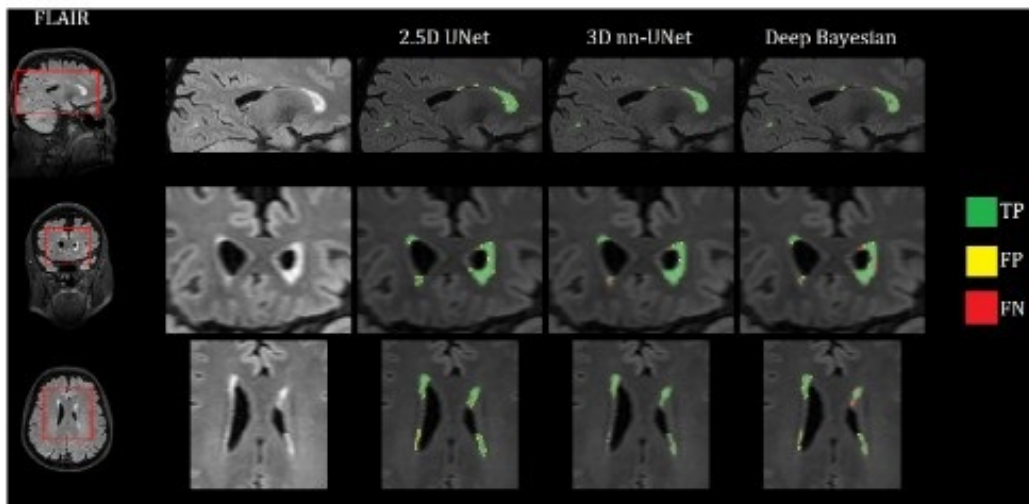
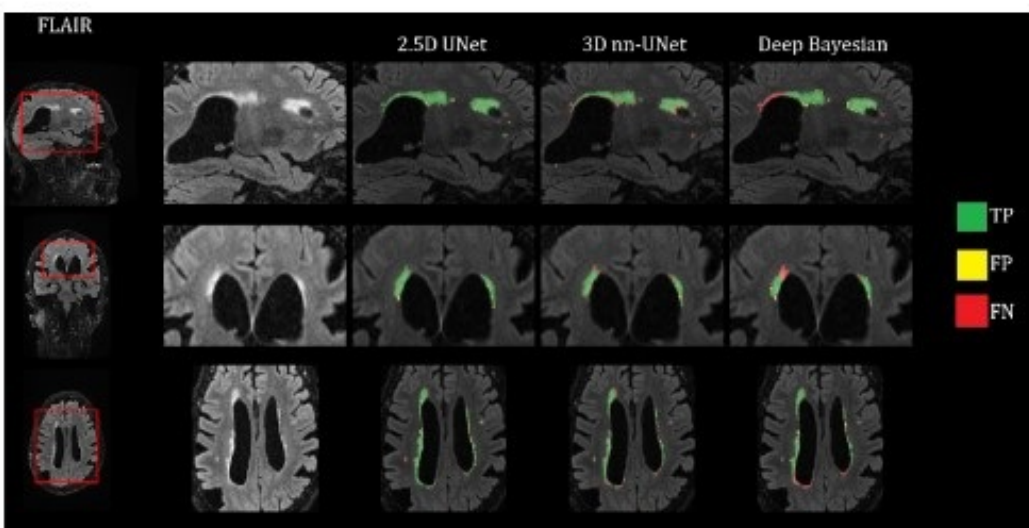


Figure 3: Boxplot of the external test data ( $n = 29$ ) performance metrics. The p-value legends are: ns:  $0.05 < p \leq 1.00$  \*:  $0.01 < p \leq 0.05$  \*\*:  $0.001 < p \leq 0.01$  \*\*\*:  $0.0001 < p \leq 0.001$  \*\*\*\*:  $p \leq 0.0001$ .

a)



b)



c)

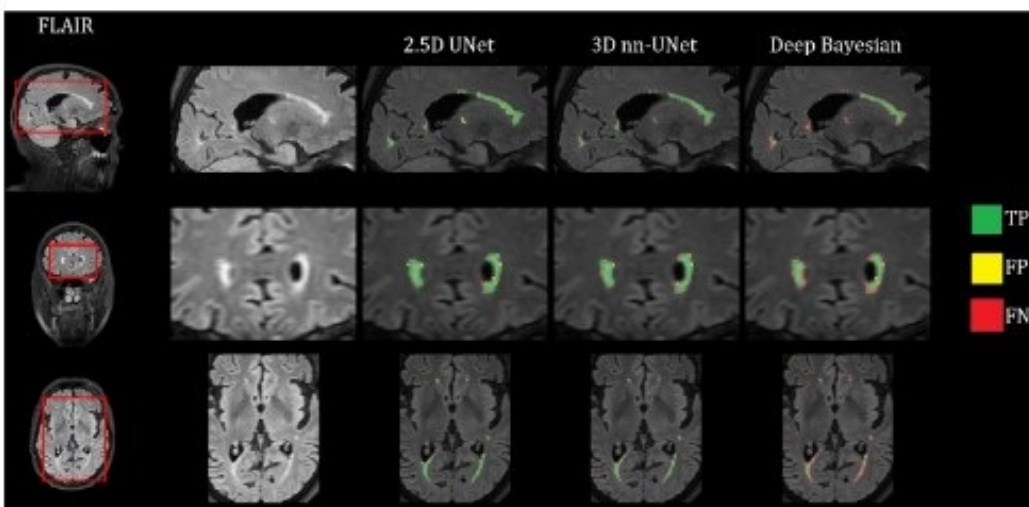


Figure 4: Example 1 of segmentations on internal test data for all three models overlaid onto FLAIR-weighted-weighted images. TP is a true positive, FP is a false positive and FN is a false negative.

Table 6: *Prediction metrics (lesion level) as a function of lesion size for the three models on the validation data. The values are shown as 2.5D U-Net/3D nnU-Net. The threshold set for true positive (TP) and false negatives (FN) is less than 50% of the lesion predicted by the model, otherwise false positive (FP).*

Lesion volume range mm <sup>3</sup>	[1, 10]	[10, 400]	[400, 1000]	[1000+ ]
Avg. Volume mm <sup>3</sup>	8/4/3	72/57/67	625/659/663	2183/2101/2450
Total	223/963/737	991/1024/621	46/45/32	33/33/32
Total TP	193/359/189	814/958/554	45/45/38	33/33/32
Total FN	826/664/834	464/320/724	0/0/7	0/0/1
Total FP	26/604/548	177/66/67	1/0/0	0/0/0
Recall	0.18/0.32/0.18	0.61/0.66/0.41	0.96/0.85/0.77	0.97/0.89/0.83

Table 7: *Performance metrics (mean +/- std.dev) for all three models in the external test dataset. \* and ^ indicate that the model performance is significantly better ( $p < 0.05$ ) compared to the 2.5D U-Net and Deep Bayesian respectively. Shown are the results from the five metrics used in the white matter hyperintensity challenge for The Medical Image Computing and Computer-Assisted Intervention Society.*

Model	DSC	HD95 [mm]	AVD [%]	Recall	$F_1$
2.5D U-Net	0.54 +/- 0.19	22.38 +/- 27.43	201.63 +/- 230.18	0.83 +/- 0.11 ^	<b>0.61 +/- 0.15 ^</b>
3D nnU-Net	<b>0.66 +/- 0.17</b> *^	14.29 +/- 12.61	58.35 +/- 78.82 *	<b>0.89 +/- 0.11</b> ^	0.56 +/- 0.12
Deep Bayesian	0.53 +/- 0.18	<b>13.41 +/- 9.45</b>	<b>48.93 +/- 41.73</b> *	0.71 +/- 0.16	0.50 +/- 0.16

Table 8: *Prediction metrics (lesion level) as a function of lesion size for the three models on the external test data. The values are shown as 2.5D U-Net/3D nnU-Net/Deep Bayesian. The threshold set for true positive (TP) and false negatives (FN) is less than 50% of the lesion predicted by the model, otherwise false positive (FP).*

Lesion volume range mm <sup>3</sup>	[1, 10]	[10, 400]	[400, 1000]	[1000+ ]
Avg. Volume mm <sup>3</sup>	8/4/3	71/53/77	640/601/582	3704/2694/2436
Total	33/391/380	610/523/283	17/16/14	19/18/16
Total TP	14/14/4	351/326/203	16/16/14	18/18/16
Total FN	26/26/36	69/94/217	0/0/2	0/0/2
Total FP	19/377/376	259/197/80	1/0/0	1/0/0
Recall	0.31/0.32/0.11	0.78/0.67/0.45	0.98/0.89/0.75	0.98/0.88/0.73

cohorts, yielding inferior results, and are not applying deep learning-based methods.

The Deep Bayesian model was trained on combined imaging features from 3D T1- and 2D FLAIR-weighted images; whereas, the two in-house models were trained exclusively using the 3D FLAIR-weighted images.

From a clinical perspective, it is appealing to produce an automated WMH segmentation using only one MRI sequence, obviating new quality control and/or co-register multiple image inputs, while also reducing complexity and barriers to adoption in a clinical setting.

The 2.5D and the 3D U-Net models performed favorably in comparison with the reference SOTA Deep Bayesian model in the external test set. Overall, the in-house trained 3D nnU-Net model had the best performance across all of the test metrics.

As expected, the performance of all three models was strongly dependent on lesion size, with a rapid drop in performance for individual lesion volumes less than 10 mm<sup>3</sup>. The reason for the low Recall and F1 scores in the

smallest lesions is the severe penalty for just misclassifying a few voxels.

Although detecting tiny lesions is of interest and potentially clinically meaningful, we chose to focus on volumes that were nominally larger than a minimum volume primarily because very small suspected lesions will obfuscate the test performance measures. As a side note, it would be interesting to have a model that looked at tiny lesions by potentially using higher resolution MRI.

Interestingly, the reference model performance was inferior for all metrics in our test data compared to the previously published test results in the Deep Bayesian study. A DSC of 0.63 (+/- 0.15) was obtained in our study, compared to the previously reported value of 0.893 (+/- 0.08). It should be stated that the reference model was not re-trained.

However, these performance differences highlight the need for broad and diverse deep learning model training[40]. It is also worth mentioning that the in-house trained models had in excess of 7 M parameters whereas the Deep Bayesian model only has 515 K parameters. One may be expected that models with more parameters should be able

to learn more subtle image features, but could also make them more susceptible to overfitting.

It would be interesting to increase the number of parameters in the Deep Bayesian, given its already good performance in the current form. The Deep Bayesian also generates an uncertainty map that can be very useful for further analysis.

An ensemble of the two in-house models could be developed to get similar uncertainty maps, which will be attempted in ongoing work. The two in-house models were trained exclusively on 3D FLAIR-weighted data and this matched the details of the test data.

This may explain the better performance of these models. Conversely, these results may suggest that our models would perform less well in 2D anisotropic FLAIR data. However, since our aim was specifically to develop models with optimal performance in the 3D FLAIR series, potentially poorer performance in 2D data was of less concern.

Although the test sets were acquired with a similar 3D FLAIR-weighted protocol as the training data using the same MRI system as one of the national sites, some clear differences in the intra-scanner distributions. The external test dataset only contained images from a single Prisma scanner, while the training data only included 29 cases from Prisma.

The lack of training cases from this scanner type may explain the reduced model performance for the external dataset. A potential remedy for such large variations in intensity distributions could be to apply an adaptive histogram normalization method as part of the pre-processing procedure[41] or to apply a brain extraction algorithm to remove non-brain tissue from the analysis[33][42].

This was not performed in our study as we wanted to avoid excessive pre-processing requirements. The results with all three models were, on average, inferior to the results from the best model in the MICCAI WMH challenge.

However, since the models tested here were not trained on the MICCAI dataset, a direct comparison of performance may be misleading. It is also worth mentioning that the nnU-Net framework was optimized in its default configuration, significantly reducing training time compared to the 2.5D U-Net model.

## 5 Limitations

The study has limitations. First, although the in-house developed models were trained on a large dataset (. n=642 participants across five national sites and six scanner types), the test sets of n=60 (internal) and n=29 (external) were modestly sized.

Ultimately these sample sizes reflect a degree of pragmatism to train, evaluate, and deploy models while recognizing the bottleneck of performing 671 ground truth segmentations. Second, the in-house models were only

trained on FLAIR-weighted data whereas the reference model was trained on a combination of FLAIR-weighted and T1-weighted data.

Our results do, however, suggest that T1-weighted images may not be needed for WMH segmentation, however, more explicit work on this is warranted. Third, the 3D nnU-Net used a pre-defined method of splitting the data into training and validation sets, causing the training/validation samples to be slightly different compared to the 2.5D U-Net, but it does have the same training data size.

We do not expect this to have had a major impact on performance differences. Fourth, the test and validation data were not annotated manually from scratch. Rather, annotations were based on segmentation using an established non-CNN-based algorithm, which was then reviewed and approved by one or two domain experts for the final ground truth.

Given a large amount of data in the 3D series (> 200 slices per 3D FLAIR volume), fully manual annotation of the complete test dataset was not feasible in our current setup. Finally, the models investigated have not yet been used prospectively, therefore it remains to be determined whether these Artificial intelligence (AI) tools can be used across a wide range of brain diseases. This will be the important final step in investigating clinical utility, and whether this is a robust tool for widespread national use in ongoing national AD MRI studies.

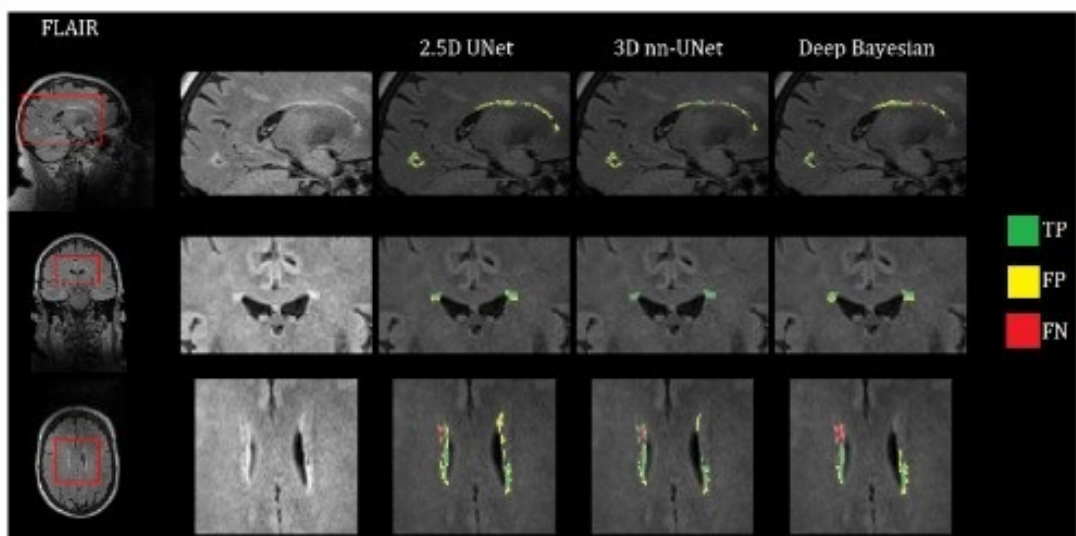
There is also some consideration that has to be taken into account when comparing the in-house trained models with the reference model. Making a direct comparison between the in-house and external models is not fair as they are not trained on the same data. The reason for including it is to check the difference between off-the-shelf trained models against in-house trained models, in an effort to see the generalizability of SOTA level models.

## 6 Conclusion

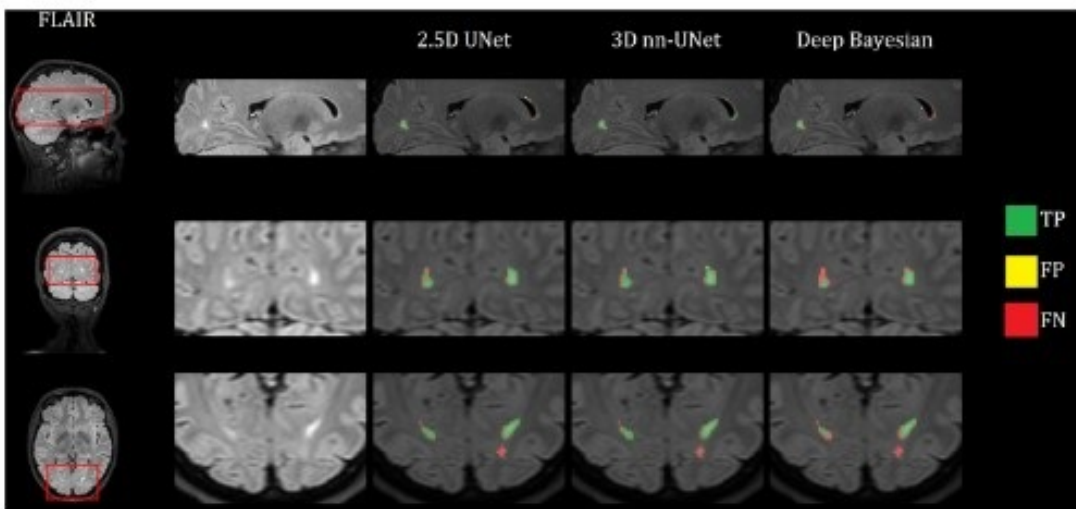
Automated and robust WMH segmentation was obtained using 3D FLAIR-weighted images acquired at both 1.5T and 3T. With the increasing use of 3D FLAIR-weighted images in MRI protocols, our results suggest that WMH segmentation models can be trained on 3D data and yield WMH segmentation performance that is comparable to or better than SOTA without the need for including T1-weighted image series.

The 3D nnU-Net gave the overall best performance and will be used for further testing on new data and automating WMH segmentation in our ongoing AD-related research activities.

a)



b)



c)

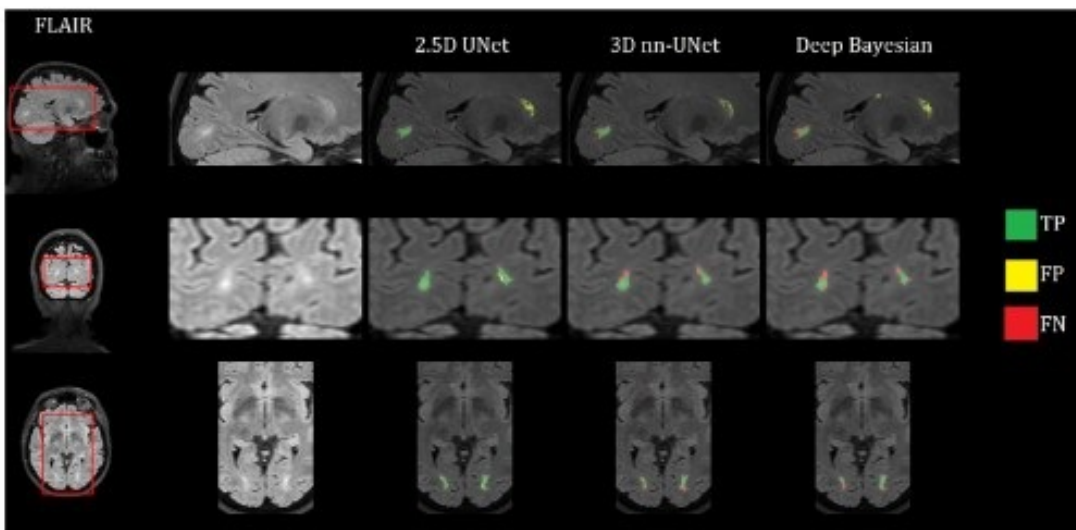


Figure 5: Example 2 segmentations on the internal test data for all three models overlayed on FLAIR-weighted. TP is a true positive, FP is a false positive and FN is a false negative.

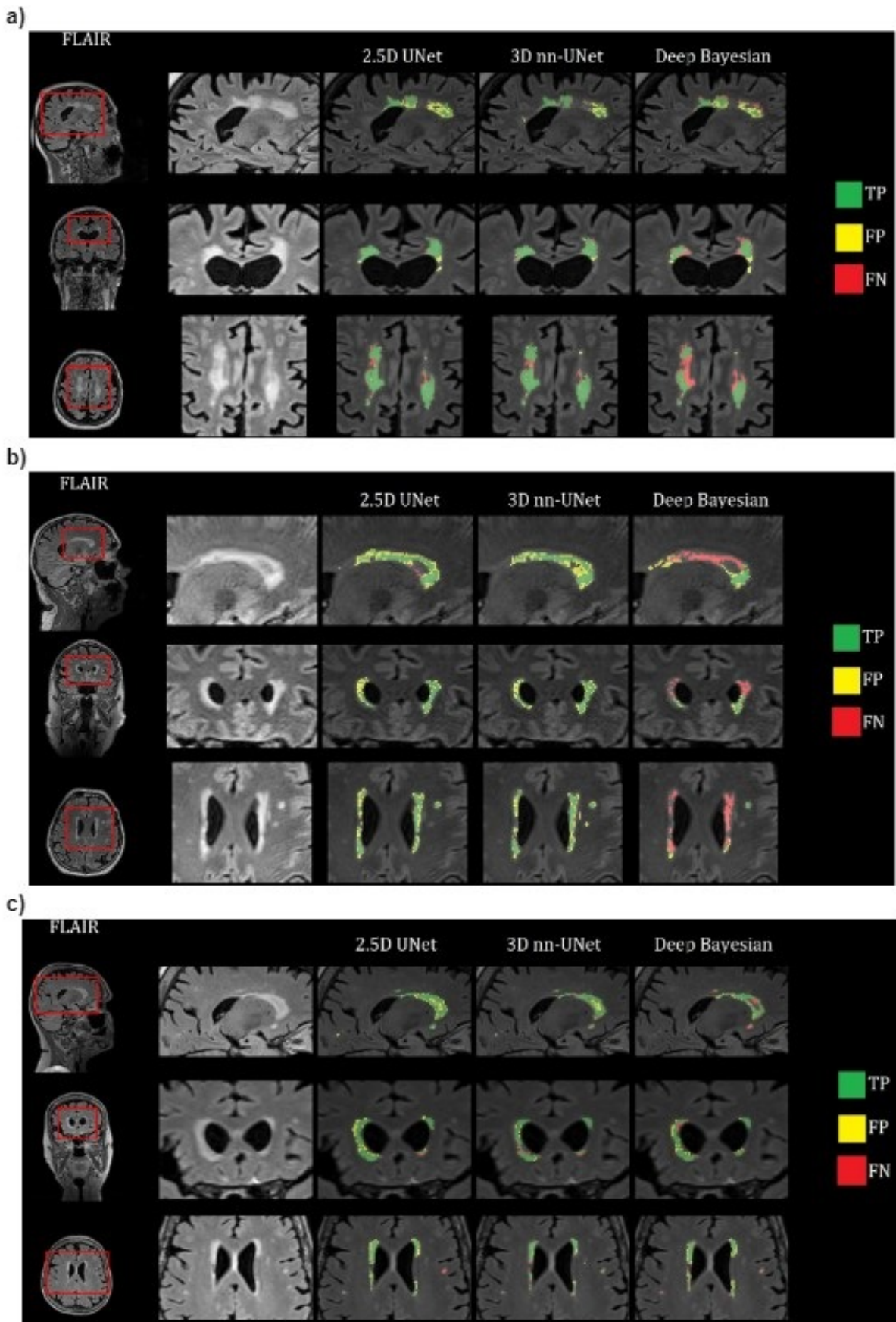


Figure 6: Example segmentations of external test data for all three models overlayed on FLAIR-weighted. TP is a true positive, FP is a false positive and FN is a false negative.

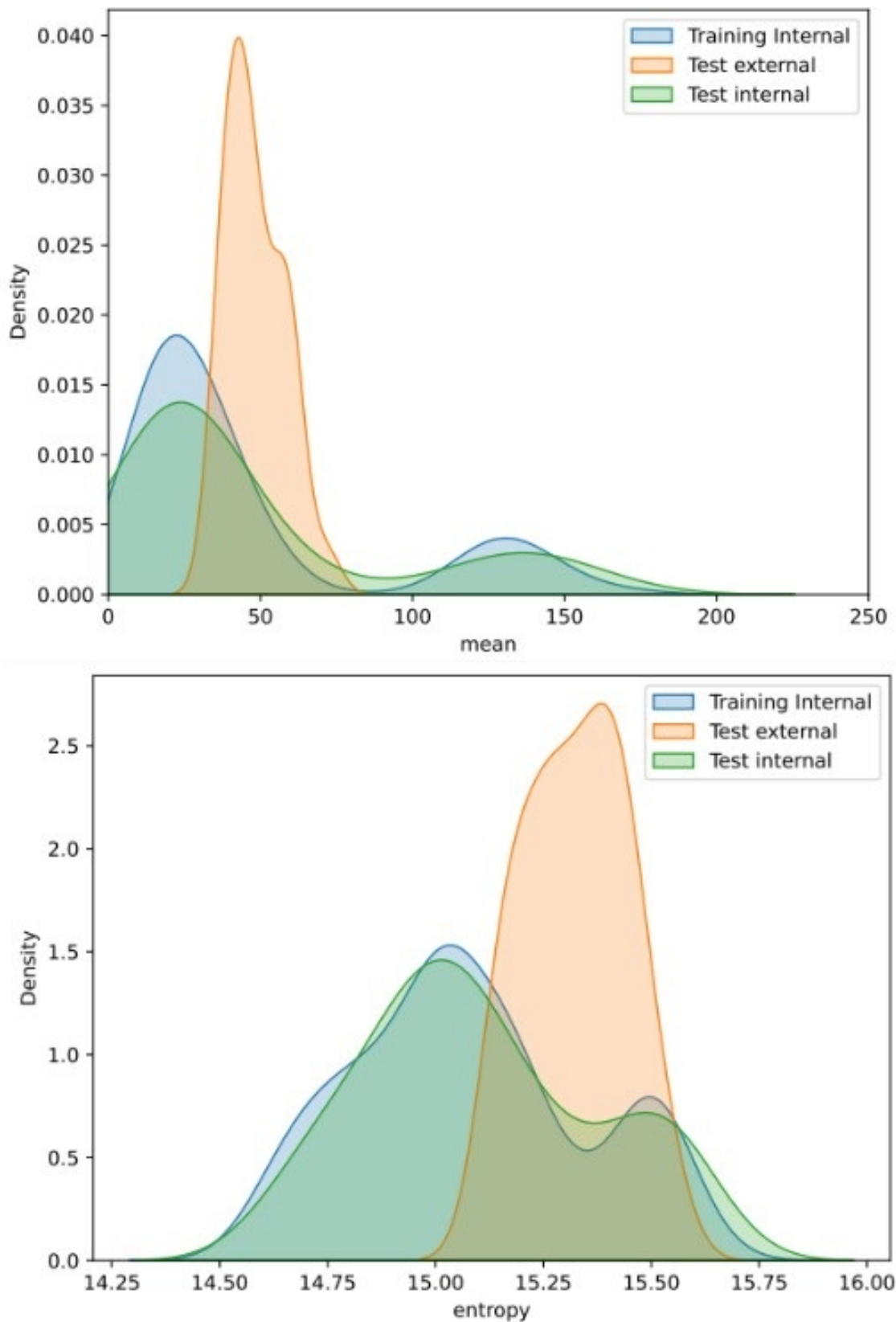


Figure 7: Histogram of the FLAIR-weighted MRI image intensity means and intensity entropy across all image volumes in their respective data sets. Note the large deviation the distributions for the external test data compared to the training and internal test data.

## References

[1] Clifford R Jack, David S Knopman, William J Jagust, Ronald C Petersen, Michael W Weiner, Paul S Aisen, Leslie M Shaw, Prashanthi Vemuri, Heather J Wiste, Stephen D Weigand, Timothy G Lesnick, Vernon S Pankratz, Michael C Donohue, and John Q Trojanowski. Tracking pathophysiological processes in alzheimer's disease: an updated hypothetical model of dynamic biomarkers, 2013.

[2] Raffaella Valenti. *Cerebral Small Vessel Disease and Cerebral Amyloid Angiopathy: Neuroimaging markers, cognitive features and rehabilitative issues*. Firenze University Press, 2018.

[3] Joanna M Wardlaw, Eric E Smith, Geert J Biesels, Charlotte Cordonnier, Franz Fazekas, Richard Frayne, Richard I Lindley, John T O'Brien, Frederik Barkhof, Oscar R Benavente, Sandra E Black, Carol Brayne, Monique Breteler, Hugues Chabriat, Charles Decarli, Frank-Erik de Leeuw, Fergus Doubal, Marco Duering, Nick C Fox, Steven Greenberg, Vladimir Hachinski, Ingo Kilimann, Vincent Mok, Robert van Oostenbrugge, Leonardo Pantoni, Oliver Speck, Blossom C M Stephan, Stefan Teipel, Anand Viswanathan, David Werring, Christopher Chen, Colin Smith, Mark van Buchem, Bo Norrving, Philip B Gorelick, Martin Dichgans, and STandards for ReportIng Vascular changes on nEuroimaging (STRIVE v1). Neuroimaging standards for research into small vessel disease and its contribution to ageing and neurodegeneration. *Lancet Neurol.*, 12(8):822–838, August 2013.

[4] Seonjoo Lee, Fawad Viqr, Molly E Zimmerman, Atul Narkhede, Giuseppe Tosto, Tammie L S Benninger, Daniel S Marcus, Anne M Fagan, Alison Goate, Nick C Fox, Nigel J Cairns, David M Holtzman, Virginia Buckles, Bernardino Ghetti, Eric McDade, Ralph N Martins, Andrew J Saykin, Colin L Masters, John M Ringman, Natalie S Ryan, Stefan Förster, Christoph Laske, Peter R Schofield, Reisa A Sperling, Stephen Salloway, Stephen Correia, Clifford Jack, Michael Weiner, Randall J Bateman, John C Morris, Richard Mayeux, Adam M Brickman, and for the Dominantly Inherited Alzheimer Network. White matter hyperintensities are a core feature of alzheimer's disease: Evidence from the dominantly inherited alzheimer network, 2016.

[5] Stéphanie Debette and H S Markus. The clinical importance of white matter hyperintensities on brain magnetic resonance imaging: systematic review and meta-analysis. *BMJ*, 341:c3666, July 2010.

[6] Xiaoxuan Liu, Livia Faes, Aditya U Kale, Siegfried K Wagner, Dun Jack Fu, Alice Bruynseels, Thushika Mahendiran, Gabriella Moraes, Mohith Shamdas, Christoph Kern, Joseph R Ledسام, Martin K Schmid, Konstantinos Balaskas, Eric J Topol, Lucas M Bachmann, Pearse A Keane, and Alastair K Denniston. A comparison of deep learning performance against health-care professionals in detecting diseases from medical imaging: a systematic review and meta-analysis. *Lancet Digit Health*, 1(6):e271–e297, October 2019.

[7] Xinxin Li, Yu Zhao, Jiyang Jiang, Jian Cheng, Wanlin Zhu, Zhenzhou Wu, Jing Jing, Zhe Zhang, Wei Wen, Perminder S Sachdev, Yongjun Wang, Tao Liu, and Zixiao Li. White matter hyperintensities segmentation using an ensemble of neural networks. *Hum. Brain Mapp.*, 43(3):929–939, February 2022.

[8] Hugo J Kuijf, Adria Casamitjana, D Louis Collins, Mahsa Dadar, Achilleas Georgiou, Mohsen Ghafoorian, Dakai Jin, April Khademi, Jesse Knight, Hongwei Li, and Et al. Standardized assessment of automatic segmentation of white matter hyperintensities and results of the WMH segmentation challenge. *IEEE Trans. Med. Imaging*, 38(11):2556–2568, November 2019.

[9] Tormod Fladby, Lene Pålhaugen, Per Selnæs, Knut Waterloo, Geir Bråthen, Erik Hessen, Ina Selseth Almdahl, Kjell-Arne Arntzen, Eirik Auning, Carl Fredrik Eliassen, Ragna Espenes, Ramune Grambaite, Gøril Rolfseng Grøntvedt, Krisztina Kunzszt Johansen, Stein Harald Johnsen, Lisa Flem Kalheim, Bjørn-Eivind Kirsebom, Kai Ivar Müller, Arne Exner Nakling, Arvid Rongve, Sigrid Botne Sando, Nikias Siafarikas, Ane Løvli Stav, Sandra Tecelao, Santiago Timon, Svein Ivar Bekkelund, and Dag Aarsland. Detecting At-Risk alzheimer's disease cases, 2017.

[10] Parisa Mojiri Forooshani, Mahdi Biparva, Emmanuel E Ntiri, Joel Ramirez, Lyndon Boone, Melissa F Holmes, Sabrina Adamo, Fuqiang Gao, Miracle Ozzoode, Christopher J M Scott, Dar Dowlatshahi, Jane M Lawrence-Dewar, Donna Kwan, Anthony E Lang, Karine Marcotte, Carol Leonard, Elizabeth Rochon, Chris Heyn, Robert Bartha, Stephen Strother, Jean-Claude Tardif, Sean Symons, Mario Masellis, Richard H Swartz, Alan Moody, Sandra E Black, and Maged Goubran. Deep bayesian networks for uncertainty estimation and adversarial resistance of white matter hyperintensity segmentation. *Hum. Brain Mapp.*, January 2022.

[11] Lene Pålhaugen, Carole H Sudre, Sandra Tecelao, Arne Nakling, Ina S Almdahl, Lisa F Kalheim, M Jorge Cardoso, Stein H Johnsen, Arvid Rongve, Dag Aarsland, Atle Bjørnerud, Per Selnæs, and Tormod Fladby. Brain amyloid and vascular risk are related to distinct white matter hyperintensity patterns. *J. Cereb. Blood Flow Metab.*, 41(5):1162–1174, May 2021.

[12] M Jorge Cardoso, Marc Modat, Robin Wolz, Andrew Melbourne, David Cash, Daniel Rueckert, and Sébastien Ourselin. Geodesic information flows: Spatially-Variant graphs and their application to seg-

mentation and fusion. *IEEE Trans. Med. Imaging*, 34(9):1976–1988, September 2015.

[13] Martin Soria Røvang. *DEEP LEARNING-BASED SEGMENTATION OF WHITE MATTER HYPERINTENSITIES IN MAGNETIC RESONANCE IMAGES: AN EARLY MARKER FOR DEVELOPMENT OF ALZHEIMER’S DISEASE*. PhD thesis, 2021.

[14] Fabian Isensee, Paul F Jaeger, Simon A A Kohl, Jens Petersen, and Klaus H Maier-Hein. nnU-Net: a self-configuring method for deep learning-based biomedical image segmentation, 2021.

[15] Olaf Ronneberger, Philipp Fischer, and Thomas Brox. U-Net: Convolutional networks for biomedical image segmentation. *CoRR*, abs/1505.04597, 2015.

[16] Diganta Misra. Mish: A self regularized Non-Monotonic neural activation function. *CoRR*, abs/1908.08681, 2019.

[17] Matthew D Zeiler, Dilip Krishnan, Graham W Taylor, and Rob Fergus. Deconvolutional networks, 2010.

[18] Adam Paszke, Sam Gross, Francisco Massa, Adam Lerer, James Bradbury, Gregory Chanan, Trevor Killeen, Zeming Lin, Natalia Gimelshein, Luca Antiga, Alban Desmaison, Andreas Köpf, Edward Yang, Zach DeVito, Martin Raison, Alykhan Tejani, Sasank Chilamkurthy, Benoit Steiner, Lu Fang, Junjie Bai, and Soumith Chintala. Pytorch: An imperative style, high-performance deep learning library, 2019. URL <https://arxiv.org/abs/1912.01703>.

[19] MONAI Consortium. MONAI: Medical open network for AI, 2022.

[20] nnU-Net for PyTorch. [https://catalog.ngc.nvidia.com/orgs/nvidia/resources/nunet\\_for\\_pytorch](https://catalog.ngc.nvidia.com/orgs/nvidia/resources/nunet_for_pytorch), . Accessed: 2022-7-11.

[21] Keras: the python deep learning API. <https://keras.io/>, . Accessed: 2022-7-11.

[22] Martín Abadi, Paul Barham, Jianmin Chen, Zhifeng Chen, Andy Davis, Jeffrey Dean, Matthieu Devin, Sanjay Ghemawat, Geoffrey Irving, Michael Isard, Manjunath Kudlur, Josh Levenberg, Rajat Monga, Sherry Moore, Derek G Murray, Benoit Steiner, Paul Tucker, Vijay Vasudevan, Pete Warden, Martin Wicke, Yuan Yu, and Xiaoqiang Zheng. TensorFlow: A system for large-scale machine learning. 2016.

[23] Nicholas J Tustison, Brian B Avants, Philip A Cook, Yuanjie Zheng, Alexander Egan, Paul A Yushkevich, and James C Gee. N4ITK: improved N3 bias correction. *IEEE Trans. Med. Imaging*, 29(6):1310–1320, June 2010.

[24] Charles R Harris, K Jarrod Millman, St’efan J van der Walt, Ralf Gommers, Pauli Virtanen, David Cournapeau, Eric Wieser, Julian Taylor, Sebastian Berg, Nathaniel J Smith, Robert Kern, Matti Picus, Stephan Hoyer, Marten H van Kerkwijk, Matthew Brett, Allan Haldane, Jaime Fernández del Río, Mark Wiebe, Pearu Peterson, Pierre Gérard-Marchant, Kevin Sheppard, Tyler Reddy, Warren Weckesser, Hameer Abbasi, Christoph Gohlke, and Travis E Oliphant. Array programming with NumPy. *Nature*, 585(7825):357–362, September 2020.

[25] Jeff Reback, jbrockmendel, Wes McKinney, Joris Van den Bossche, Matthew Roeschke, Tom Augspurger, Simon Hawkins, Phillip Cloud, gfyoung, Sinhrks, Patrick Hoefer, Adam Klein, Terji Petersen, Jeff Tratner, Chang She, William Ayd, Shahar Naveh, J H M Darbyshire, Richard Shadrach, Marc Garcia, Jeremy Schendel, Andy Hayden, Daniel Saxon, Marco Edward Gorelli, Fangchen Li, Torsten Wörtwein, Matthew Zeitlin, Vytautas Jancauskas, Ali McMaster, and Thomas Li. pandas-dev/pandas: Pandas 1.4.3, 2022.

[26] L O Wahlund, F Barkhof, F Fazekas, L Bronge, M Augustin, M Sjögren, A Wallin, H Ader, D Leys, L Pantoni, F Pasquier, T Erkinjuntti, P Scheltens, and European Task Force on Age-Related White Matter Changes. A new rating scale for age-related white matter changes applicable to MRI and CT. *Stroke*, 32(6):1318–1322, June 2001.

[27] Stefan Van der Walt, Johannes L Schönberger, Juan Nunez-Iglesias, François Boulogne, Joshua D Warner, Neil Yager, Emmanuelle Gouillart, and Tony Yu. scikit-image: image processing in python. *PeerJ*, 2:e453, 2014.

[28] Maged Goubran, Emmanuel Edward Ntiri, Hassan Akhavein, Melissa Holmes, Sean Nestor, Joel Ramirez, Sabrina Adamo, Miracle Ozzoode, Christopher Scott, Fuqiang Gao, Anne Martel, Walter Swardfager, Mario Masellis, Richard Swartz, Bradley MacIntosh, and Sandra E Black. Hippocampal segmentation for brains with extensive atrophy using three-dimensional convolutional neural networks. *Hum. Brain Mapp.*, 41(2):291–308, February 2020.

[29] Nabila Abraham and Naimul Mefraz Khan. A novel focal tversky loss function with improved attention U-Net for lesion segmentation. *CoRR*, abs/1810.07842, 2018.

[30] Diederik P Kingma and Jimmy Ba. Adam: A method for stochastic optimization, 2017.

[31] S K Warfield, K H Zou, and W M Wells. Simultaneous truth and performance level estimation (STAPLE): an algorithm for the validation of image segmentation. *IEEE Trans. Med. Imaging*, 23(7):903–921, 2004.

[32] Karen Simonyan and Andrew Zisserman. Very deep convolutional networks for Large-Scale image recognition, 2015.

[33] Fabian Isensee, Marianne Schell, Irada Pflueger, Gianluca Brugnara, David Bonekamp, Ulf Neuberger, Antje Wick, Heinz-Peter Schlemmer, Sabine Heiland, Wolfgang Wick, Martin Bendszus, Klaus H Maier-Hein, and Philipp Kickingereder. Automated brain

extraction of multisequence MRI using artificial neural networks. *Hum. Brain Mapp.*, 40(17):4952–4964, December 2019.

[34] Thorvald Sørensen. *A Method of Establishing Groups of Equal Amplitude in Plant Sociology Based on Similarity of Species Content and Its Application to Analyses of the Vegetation on Danish Commons*. 1948.

[35] R Tyrrell Rockafellar and Roger J-B Wets. *Variational Analysis*. Springer Science & Business Media, July 2009.

[36] F Ceragioli, A Dontchev, H Furuta, K Marti, and L Pandolfi. *System Modeling and Optimization: Proceedings of the 22nd IFIP TC7 Conference held from July 18-22, 2005, Turin, Italy*. Springer, June 2006.

[37] Abdel Aziz Taha and Allan Hanbury. Metrics for evaluating 3D medical image segmentation: analysis, selection, and tool. *BMC Med. Imaging*, 15:29, August 2015.

[38] Yi Zhong, David Utriainen, Ying Wang, Yan Kang, and E Mark Haacke. Automated white matter hyperintensity detection in multiple sclerosis using 3D T2 FLAIR. *Int. J. Biomed. Imaging*, 2014:239123, July 2014.

[39] Rita Simões, Christoph Mönninghoff, Martha Dlugaj, Christian Weimar, Isabel Wanke, Anne-Marie van Cappellen van Walsum, and Cornelis Slump. Automatic segmentation of cerebral white matter hyperintensities using only 3D FLAIR images. *Magn. Reson. Imaging*, 31(7):1182–1189, September 2013.

[40] Alexander D’Amour, Katherine Heller, Dan Moldovan, Ben Adlam, Babak Alipanahi, Alex Beutel, Christina Chen, Jonathan Deaton, Jacob Eisenstein, Matthew D Hoffman, Farhad Hormozdiari, Neil Houlsby, Shaobo Hou, Ghassen Jerfel, Alan Karthikesalingam, Mario Lucic, Yian Ma, Cory McLean, Diana Mincu, Akinori Mitani, Andrea Montanari, Zachary Nado, Vivek Natarajan, Christopher Nielson, Thomas F Osborne, Rajiv Raman, Kim Ramasamy, Rory Sayres, Jessica Schrouff, Martin Seneviratne, Shannon Sequeira, Harini Suresh, Victor Veitch, Max Vladymyrov, Xuezhi Wang, Kellie Webster, Steve Yadlowsky, Taedong Yun, Xiaohua Zhai, and D Sculley. Underspecification presents challenges for credibility in modern machine learning. 2020.

[41] Xiaofei Sun, Lin Shi, Yishan Luo, Wei Yang, Hongpeng Li, Peipeng Liang, Kuncheng Li, Vincent C T Mok, Winnie C W Chu, and Defeng Wang. Histogram-based normalization technique on human brain magnetic resonance images from different acquisitions. *Biomed. Eng. Online*, 14:73, July 2015.

[42] Marcela de Oliveira, Marina Piacenti-Silva, Fernando Coronetti Gomes da Rocha, Jorge Manuel Santos, Jaime Dos Santos Cardoso, and Paulo Noronha Lisboa-Filho. Lesion volume quantification using two convolutional neural networks in MRIs of multiple sclerosis patients. *Diagnostics (Basel)*, 12(2), January 2022.